Published in final edited form as:
Nanomedicine (Lond). 2013 January ; 8(1): 29–41. doi:10.2217/nnm.12.98.

The effect of cell-cluster size on intracellular nanoparticle-mediated hyperthermia: is it possible to treat microscopic tumors?

Mohammad Hedayati[1], **Owen Thomas**[1], **Budri Abubaker-Sharif**[1], **Haoming Zhou**[1], **Christine Cornejo**[1], **Yonggang Zhang**[1], **Michele Wabler**[1], **Jana Mihalic**[2], **Cordula Gruettner**[3], **Fritz Westphal**[3], **Alison Geyh**[2], **Theodore I Deweese**[1], and **Robert Ivkov**[1,*]

[1]Department of Radiation Oncology and Molecular Radiation Sciences, Johns Hopkins University School of Medicine, Baltimore, MD 21231, USA

[2]Department of Environmental Health Sciences, Johns Hopkins Bloomberg School of Public Health, Baltimore, MD 21205, USA

[3]Micromod Partikeltechnologie GmbH, Rostock, Germany

Abstract

Aim—To compare the measured surface temperature of variable size ensembles of cells heated by intracellular magnetic fluid hyperthermia with heat diffusion model predictions.

Materials & methods—Starch-coated Bionized NanoFerrite (Micromod Partikeltechnologie GmbH, Rostock, Germany) iron oxide magnetic nanoparticles were loaded into cultured DU145 prostate cancer cells. Cell pellets of variable size were treated with alternating magnetic fields. The surface temperature of the pellets was measured *in situ* and the associated cytotoxicity was determined by clonogenic survival assay.

Results & conclusion—For a given intracellular nanoparticle concentration, a critical minimum number of cells was required for cytotoxic hyperthermia. Above this threshold, cytotoxicity increased with increasing cell number. The measured surface temperatures were consistent with those predicted by a heat diffusion model that ignores intercellular thermal barriers. These results suggest a minimum tumor volume threshold of approximately 1 mm^3, below which nanoparticle-mediated heating is unlikely to be effective as the sole cytotoxic agent.

*Author for correspondence: Tel.: +1 443 287 7282, rivkov1@jhmi.edu.

Disclaimer

The contents of this article is solely the responsibility of the authors and does not necessarily represent the official views of the National Cancer Institute or the National Institutes of Health.

Financial & competing interests disclosure

C Gruettner and F Westphal are employees of micromod Partikeltechnologie, GmbH, manufacturer of the particles used in this study. This work was supported by an award from the Prostate Cancer Foundation/Safeway Foundation (STAR), and by Award Number U54CA143803 from the National Cancer Institute. Inductively coupled plasma mass spectrometry work was supported in part by the Maryland Cigarette Restitution Fund Program at Johns Hopkins Bloomberg School of Public Health and the NIEHS Center P30 ES00319. The authors have no other relevant affiliations or financial involvement with any organization or entity with a financial interest in or financial conflict with the subject matter or materials discussed in the manuscript apart from those disclosed.
No writing assistance was utilized in the production of this manuscript.

Keywords

alternating magnetic field; cancer therapy; hyperthermia; intracellular; iron oxide; magnetic nanoparticles

Background

In 1979, Gordon *et al.* hypothesized that cell membranes are effective thermal insulators, capable of retaining heat and thus enabling a significant elevation of the cytoplasmic temperature [1]. Consequently, according to Gordon, intracellular thermal therapy is likely to be therapeutically superior to its extracellular counterpart. This hypothesis implies that therapeutic hyperthermia may be achievable in a single tumor cell. Indeed, this is the basis for pursuing intracellular hyperthermia as a strategy for treating microscale metastatic cancer [2,3].

Gordon's hypothesis was based on his experimental work employing phagocytized and magnetically excitable particles, the precursors of contemporary magnetic nanoparticles. Magnetic nanoparticles generate heat when exposed to alternating magnetic fields (AMFs), and biocompatible suspensions of magnetic nanoparticles have the potential to deliver heat selectively to tumors for cancer therapy [4–6]. The thermal dose delivered is a function of the concentration of magnetic nanoparticles in tissue, their heating efficiency at the AMF conditions employed [7] and the duration of AMF application.

A significant body of theoretical work questions the hypothesis that intracellular nanoparticle-based hyperthermia is potentially effective and achievable for small systems including individual cells [8–13]. Central to this work is the nature of diffusive heat transfer, which diminishes the ability of a heated object to achieve and sustain a high temperature as its surface area (and thus area for heat exchange) to volume ratio increases. As a consequence, small objects (such as single cells) exhibit smaller temperature rises than larger objects (such as pellets of cells) when both are heated by equivalent loss power densities (W/cm^3). It should be noted that these theoretical studies typically do not consider the cell membrane to provide a significant barrier to diffusive heat transfer.

Rabin employed a simple diffusive heat transfer model to predict that the maximum temperature change incurred by an isolated cell is negligible, even if the cells are packed to capacity with AMF-treated magnetic nanoparticles [8]. Furthermore, he integrated experimentally achievable intracellular nanoparticle concentrations and heating efficiencies (150 W/g Fe for iron oxide nanoparticles at 500 pg Fe/cell) to predict the achievable steady-state temperature increase of collections of such cells. He determined that a large collection of nanoparticle-containing cells, approximately 1 mm in diameter or containing approximately 200,000 cells, would be necessary for therapeutic levels of hyperthermia to be achieved. Theoretical analyses by Hergt and Dutz [10], Keblinski *et al.* [11], Yamada *et al.* [12] and Kalambur *et al.* [9] have been consistent with this finding.

Here we employ a simple experimental model to investigate the size dependence of hyperthermia mediated by intracellular AMF-treated nanoparticles. We demonstrate that the achievable steady-state surface temperature of a collection of AMF-treated, nanoparticle-containing cells increases with the size of that collection and is well predicted by a simple heat diffusion model. We explicitly demonstrate that for smaller collections of cells, not only does the achievable steady-state surface temperature decrease as predicted, but the associated hyperthermia-mediated cytotoxicity diminishes as well, becoming negligible in small, submillimeter systems.

Materials & methods

Experimental design

An overview schematic of the experimental design is provided in Figure 1 to illustrate the experimental procedure and is summarized here for clarity. Each step is described in detail below. Cells were cultured and exposed to iron oxide magnetic nanoparticles that were modified to enhance cellular internalization of the particles. After allowing sufficient time to internalize the particles, cells were harvested and washed to remove loose particles from the cellular milieu. This was followed by centrifugation at a constant speed to form cell pellets with consistent cell-packing density. The pellets were then placed in the AMF coil and exposed to constant field intensity for a continual time. The surface temperature of the pellets was measured and cells were assayed for cytotoxic response using clonogenic assay. Results obtained from these experiments are compared against theoretical predictions and discussed.

Characterization of nanoparticles Size & ζ-potential

Suspensions of starch-coated magnetite (Fe_3O_4) core shell particles (Bionized NanoFerrite [BNF], catalog no. 10-00-102) were obtained from Micromod Partikeltechnologie GmbH (Rostock, Germany). Synthesis procedure and structural and magnetic properties of these particles have been described elsewhere [14,15], and a summary is provided here. These nanoparticles were produced by precipitating ferric and ferrous sulfate salts from solution with high pH in a high-pressure homogenization reaction vessel [14]. The iron content was provided by the manufacturer and was reported to be >70% w/w, with a total iron concentration of approximately 30 mg Fe/ml (42 mg particle/ml). The particles were suspended in sterile water to provide a stable biocompatible suspension [14].

Size and ζ-potential measurements were performed on the samples using a Malvern Zetasizer Nano ZS-90 (Malvern Instruments Ltd, Worcestershire, UK). Photon correlation spectroscopy was used to determine the hydrodynamic particle diameter of the particle samples. Samples were diluted in sterile water to an iron concentration of approximately 0.4 mg/ml prior to analysis.

Transmission electron microscopy (TEM) was used to obtain characteristic images of each of the nanoparticles. Images were obtained using an EM 912 (Zeiss, Oberkochen, Germany) working at 100 keV. Particle solutions were diluted and spin coated onto a carbon film-coated grid to isolate individual particles for imaging.

Specific loss power characterization

The amplitude-dependent specific loss power (SLP) for each particle was estimated from measured time-dependent heating in the AMF device (described below) at several applied amplitude (V) values from 50–1200 Oe (10,000 Oe = 1 T). Sample temperatures were measured with fiber optic probes (FISO Technologies, Inc., QC, Canada). The SLP was estimated from the slope, $\Delta T/\Delta t$, of the time–temperature curve using methods described previously [16].

Briefly, a 1-ml volume of nanoparticle suspension (no cells) was placed in a standard 12-mm polystyrene test tube and inserted into the insulating sample holder. Equilibrium between the probe, sample and the calorimeter was confirmed and the AMF power was applied. Temperatures were recorded in 1-s intervals. At each power setting a sample of distilled water was measured to correct for calorimeter heat capacity.

The temperature at time interval (T_n) was subtracted from the initial temperature (T_0) to yield the net temperature change, $\Delta T_n = T_n - T_0$. In a similar manner, the net temperature change of water blank was calculated (i.e., $\Delta T_{blank} = T_{blank}(t = n) - T_{blank}(t = 0)$). The net temperature change observed in the blank water sample was subtracted from net temperature change (ΔT_n) of sample to yield the corrected temperature change for each sample. The SLP was estimated from the initial and steepest part of the slope, $\Delta T/\Delta t$, of the time–temperature curve, by fitting a linear weighted least squares function (Origin, MA, USA) to the data. The appropriate interval for calculating the slope was determined by analyzing a plot of the incremental temperature change, analogous to the first derivative of the heating rate [16].

Nanoparticle loading into cancer cells

Human prostate carcinoma DU145 cells (ATCC, VA, USA) were maintained and propagated according to the ATCC protocol. Exponentially growing cells were treated in T-75 cm^2 tissue culture flask containing GIBCO® RPMI 1640 medium (Invitrogen, CA, USA), with 10% fetal bovine serum. Variable concentrations of BNF particles and sterile poly-D-lysine (PDL; Sigma-Aldrich, MO, USA) (Table 1) were added to the medium and particle exposure was performed over time periods of 16–24 h. Extracellular particles were removed following exposure by rinsing the flask three times with Dulbecco's phosphate-buffered saline (PBS). Cells were detached by brief exposure to 0.25% trypsin EDTA and were resuspended in RPMI prior to counting.

Intracellular particle characterization Inductively coupled plasma mass spectroscopy

Subsequent to washing and trypsinization, a portion (5×10^5 to 1×10^6 cells) of the cell preparation, which was to be used in our thermal and survival studies, was again pelleted by centrifugation and stored at −20°C for further characterization by inductively coupled plasma mass spectrometry (ICP-MS). These samples were resuspended in nitric acid and thermally digested using a two stage ramp-to-temperature microwave method. A MARS5 Xpress microwave (CEM Corporation, NC, USA) was used. Digested samples were diluted for mass spectrometric evaluation and the total iron content of the samples was determined using an Agilent 7500ce ICP-MS (Agilent Technologies, CA, USA). An eight point calibration curve was performed prior to sample analysis. As demonstrated in Table 1, at least three samples were analyzed by ICP-MS for each cell preparation. The total iron content per cell was calculated, accounting for the number of cells provided as well as dilution factors, as the mean value for these samples.

TEM & light microscopy of intracellular nanoparticles

To confirm the intracellular location of the nanoparticles, DU145 cells were grown on Thermonox® coverslips (TED PELLA, Inc., CA, USA) and treated with starch-coated BNF particles and PDL as described above. They were then fixed either for light microscopy employing Prussian Blue staining or for TEM.

For light microscopy, cells were grown in chamber slides and following treatment with nanoparticles they were washed three times in PBS to remove unbound or noninternalized iron oxide particles. They were then fixed with 3% formaldehyde for 15 min at room temperature and again washed with PBS and incubated in the dark for 30 min with a 4% weight/volume solution of Prussian Blue stain, which consists of a 1:1 combination of 4% volume/volume HCl and potassium hexacyanoferrate(II). Stained cells were washed again with PBS.

For TEM, cells were fixed with a solution containing 2% glutaraldehyde, 1 M sodium cacodylate, 3% sucrose and 3 mM $CaCl_2$ pH 7.2 for 1 h at room temperature on a slow rocker. After a 30 min buffer rinse, cells were postfixed in a solution containing 1% osmium

tetroxide reduced with 0.8% potassium ferrocyanide, 0.1 M sodium cacodylate and 3 mM $CaCl_2$ at 4°C for 1 h in the dark. Samples were then rinsed with de-ionized water and en bloc stained with 2% aqueous uranyl acetate (0.22 μm filtered) for 1 h in the dark. Cell embedding and sectioning was performed per protocol and grids were examined on a Hitachi H-7600 TEM (Hitachi, Tokyo, Japan) operating at 80 kV. Images were digitally captured with an AMT HR 1K X 1K (Advanced Microscopy Techniques, FL, USA) charge-coupled device camera.

Cell pellet formation & AMF exposure

After loading the DU145 cells with nanoparticles as described above, variable numbers of the detached cells were centrifuged at 1000 rpm for 5 min to form cell pellets of variable dimensions but having consistent cell number density. All pellets were made in duplicate and maintained in a constant volume of 0.5 ml of culture media in a 5-ml tube both before and during treatment. Samples were then placed in the center of a 4-turn solenoid, which was lined with a circulating water jacket. The water jacket was maintained at 37°C, and all samples were allowed to equilibrate to this temperature prior to AMF treatment.

The AMF system has been previously described [16–19]. The AMF system comprised three main components: a power supply, an external impedance matching network and a solenoid coil. The power supply is an 80-kW induction heating system manufactured by PPECO (CA, USA) that provides an alternating current to a resonant circuit with variable frequency between 135 and 440 kHz. The external impedance match network (AMF Life Systems, Inc., MI, USA) was adjusted for stable oscillation at 150 ± 1 kHz. The 4-turn solenoid coil had an inner diameter of 45.5 mm and was constructed from dehydrated annealed soft-copper refrigerator tubing with a 6.4-mm outer diameter. Within the solenoid, a polypropylene jacket, through which distilled water was circulated, provided a thermal barrier to heat generated directly by the solenoid.

For all cell heating experiments, the AMF amplitude was fixed at 1100 Oe and cells were exposed for 30-min duration. The magnitude of the magnetic field was measured prior to cell exposure at the center of the solenoid using a magnetic field probe [16]. For each cell pellet exposed to AMF, a size-matched pellet was separately placed and maintained at 37°C within the solenoid for an equivalent 30-min period with power off (0 Oe) as a control. The surface temperature of the pellet was measured during AMF exposure by placing an RF-resistant fiber optic temperature probe (FISO Technologies) on the pellet surface. For each tube, the temperature probe was inserted through a universal cap that fit onto all tubes. The temperature probe was fixed to the cap by Parafilm® (Pechiney Plastic Packaging, IL, USA) and the same cap with probe was used for all measurements. Thus the temperature probe was positioned in about the same position relative to cell pellet for each tube/experiment.

Clonogenic survival assay

After AMF exposure the pellets were thoroughly resuspended. Cells were then diluted to the appropriate density and placed in triplicate into 100-mm culture dishes. A total of 10–14 days after AMF treatment, cells were stained with a solution of crystal violet in 50% methanol. Colonies consisting of at least 50 cells were counted. The surviving fraction was determined relative to the survival of matched pellets that were formed at the same time but were not exposed to AMF.

Theoretical modeling

The theoretical model for heating used in this work assumes a uniformly and constantly heated spherical object embedded in an infinite, homogenous medium. It assumes that there is no thermal barrier between the heated object and the medium, and that all heat transfer is

diffusion mediated. It should be noted that Rabin employed these same assumptions when theoretically addressing the achievable temperatures of a single AMF-treated nanoparticle, a single cell packed with such nanoparticles and collections of nanoparticle-containing cells [8].

The appropriate heat diffusion equations for a uniformly and constantly heated sphere of radius *R*, embedded in an infinite, homogeneous medium with no thermal barrier between sphere and medium are [20,21]:

$$\frac{1}{r^2}\frac{\partial}{\partial r}\left(r^2\frac{\partial T_s}{\partial r}\right)+\frac{P}{k_s}=\frac{1}{\alpha_s}\frac{\partial T_s}{\partial t} \quad (1)$$

for $0 \le r \le R$

$$\frac{1}{r^2}\frac{\partial}{\partial r}\left(r^2\frac{\partial T_m}{\partial r}\right)=\frac{1}{\alpha_m}\frac{\partial T_m}{\partial t} \quad (2)$$

for $r \ge R$

Here, r is the radial dimension, t is time, P is the heating rate per unit volume within the sphere, T_s is the temperature within the sphere, T_m is the temperature within the surrounding medium, k_s is the thermal conductivity of the sphere, α_s is the thermal diffusivity of the sphere and α_m is the thermal diffusivity of the medium.

As t goes to infinity, Equation 1 reduces to the following solution for the steady-state temperature distribution within the sphere [20]:

$$\Delta T_s(r)=\frac{R^2P}{k_s}\left\{\frac{1}{3}\frac{k_s}{k_m}+\frac{1}{6}\left(1-\frac{r^2}{R^2}\right)\right\} \quad (3)$$

Here, $\Delta T_s(r)$ is the change in temperature of the sphere (above the ambient temperature) as a function of radial dimension, r. Assuming that $k_s = k_m$ (in our case assuming the thermal conductivities of both the cell pellet and surrounding medium to be equivalent to that of water [$k_{water} = 0.58$ W/ m°C]), Equation 3 reduces to the following at the surface of the sphere, where $r = R$:

$$\Delta T_{surface}=\frac{D^2P}{12\,k_s} \quad (4)$$

Here, D is the diameter of the sphere. The temperature increase within the sphere is predicted to be greatest at the center, where $r = 0$. Here Equation 3 reduces to:

$$\Delta T_{center}=\frac{D^2P}{8\,k_s} \quad (5)$$

When the heat within the sphere is generated by magnetic nanoparticles having iron concentration, c (g Fe/cm^3), and SLP (W/g Fe), where SLP is the specific loss power or heating rate of the particles normalized by mass of iron, within the sphere, P is then given by:

$$P = SLP\, c \quad (6)$$

Our cell pellet volumes were obtained from the measured mean cellular diameter and cell numbers, assuming random close packing of cells. The diameters of the pellets were calculated from these volumes, and our measured intracellular iron concentrations and nanoparticle SLP allowed us to calculate a steady-state temperature increase at any radial dimension, *r,* within the pellet (Equation 3). It should be noted that the SLPs of the nanoparticles were very similar when measured either in solution (with no cells) or intracellularly, or when inside the cells (Supplementary Figure 1; see online at www.future-medicine.com/doi/full/10.2217/nnm.12.98).

Results

Physical characterization of particles

Particle sizing measurements via photon correlation spectroscopy yielded the distribution curves shown in Figure 2A. The diameters reported in Figure 2A are the Z-average values, showing a mean diameter of about 108 nm with a polydispersity index of 0.033 for particles alone. A representative TEM image of a nanoparticle core demonstrates significant shape anisotropy (Figure 2B) with a core of approximately 50 nm comprising iron oxide crystals (98% Fe_3O_4 [15]) having a mean diameter of 10–20 nm (Figure 2B). The starch coating is not typically visible with high energy electrons (100 keV), however, the proximity of the crystalline domains to one another suggests they were adherent and not merely agglomerated. These results are consistent with those previously reported for BNF nanoparticles [14–16]. Addition of the sterile PDL to the nanoparticles increases both the measured hydrodynamic diameter to about 130 nm and the polydispersity index to about 0.2 (Figure 2A). This increase of size is accompanied by an increase of the measured pH-dependent ζ-potential from a slightly negative value of −4 mV at pH 7.4 in the absence of PDL to about −2 mV at pH 7.4, a nearly neutral value in the presence of PDL (Figure 2C). PDL is a well known nonviral transfecting agent that forms a complex with negatively charged DNA molecules and enhances its cellular uptake (in part through endocytosis). It is likely that PDL interacts with nanoparticles to enhance their uptake through a similar mechanism.

Amplitude-dependent SLP results are shown in Figure 2D. The BNF particles display relatively poor heating at low amplitude with rapidly increasing heating efficiency between 300 and 800 Oe, and saturating at a maximum SLP of 480 ± 20 W/g Fe above 1000 Oe (Figure 2D). While the clinical applicability of this high AMF amplitude may be suspect, it is necessary for the current study to extract the maximum heat produced by particles in order to assess the full capability of intracellular magnetic fluid hyperthermia.

Cellular internalization of particles

A representative 40× light microscopic image of adherent cells stained with Prussian Blue following nanoparticle exposure is shown in Figure 3A. Significant deposits of ferric iron are apparent as blue regions with variable density within the cells. The presence of iron is confirmed and quantified by ICP-MS indicating a concentration-dependent association of iron with cells following incubation with increasing concentrations of nanoparticles (Table 1). In the absence of nanoparticles, the retained iron content of cells after washing is less than 0.01 pg Fe/cell corresponding to <9 nanoparticles/ cell (8.4×10^{14} nanoparticles/g Fe). This amount changes to 2.5 ± 0.6 pg Fe/cell (~2100 nanoparticles/cell) when the cells are exposed to nanoparticles in the absence of PDL, at the maximum nanoparticle concentration used (150 μg Fe/ml). With PDL, the internalization efficiency increases dramatically,

yielding a measured iron concentration of approximately 200 ± 41.5 pg Fe/cell, or an estimated 1.7×10^5 particles/cell when exposed to 150 μg Fe/ml (1.3×10^{11} particles) under the same conditions. Intracellular localization of the nanoparticles is confirmed by TEM. Representative images are shown in Figure 3B and demonstrate the intracellular localization of nanoparticles within endosomes, consistent with previously reported findings [15].

Thermometry

An example of measured cell-pellet surface temperature profile is given in Figure 4. The maximum achieved surface temperature (T_{max}) of cell pellets containing nanoparticles are given in tabular form in Table 2 (a more detailed profile of maximum surface temperatures showing variations in temperature measurements is shown in Supplementary Table 1). Here, cell pellets are described both by their cell number and intracellular iron concentration as determined by ICP-MS. The maximum increase in temperature over baseline ΔT_{max} (T_{max} −37°C) is represented graphically in Figure 5A, partitioned by intracellular iron concentration and plotted against the calculated square of the diameter of the pellets D^2, given in mm^2. Results obtained from weighted linear least squares regression are represented by dashed lines, which are overlaid on the theoretically predicted linear relationship between D^2 and $\Delta T_{surface}$ (Equation 4).

Cell survival outcomes

Cell survival fractions as a function of measured pellet surface temperature or as a function of calculated core pellet temperature are shown in Figure 5B & 5C, respectively. Cell survival as a function of number of cells, partitioned by level of iron oxide particle loading is shown in Figure 5D (matched pellets that were not treated with AMF were included for each treatment in order to adjust for non-AMF related factors such as iron toxicity). These data demonstrate that the size of the pellet (i.e., cell number) required for thermally mediated cytotoxicity decreases with increasing iron concentration. For instance, a cell pellet with an intracellular iron concentration of approximately 5 pg Fe/cell demonstrates negligible cytotoxicity even when the pellet is relatively large and comprises 3×10^6 cells. Conversely, cytotoxicity is observed in pellets containing 6×10^5 cells at an intracellular iron concentration of approximately 70 pg Fe/cell and 2.5×10^5 cells at a concentration of 200 pg Fe/cell. This relationship reflects the fact that cytotoxicity correlates with measured pellet surface temperature, regardless of pellet size or intracellular iron concentration.

Comparison to theory

For the purposes of this article, the most relevant temperatures predicted by our theoretical model are the steady-state pellet surface temperature (Equation 4) because it correlates to our measured pellet surface temperature, and the steady-state pellet center temperature (Equation 5) because it is predicted to be the highest temperature achievable within the pellet.

As demonstrated in Figure 5A, the maximum temperature change measured at the surface of each pellet ($\Delta T_{surface}$) is consistent with that predicted by Equation 4, and toxicity measured by cell survival assay is also consistent with expected thermal toxicity from measured cell-pellet surface temperature (Figure 5B). While the center or core temperature of the pellets could not be reliably measured, the strong correlation between calculated and measured $\Delta T_{surface}$ supports the hypothesis that the above expression for ΔT_{center} approximates the true maximum pellet center temperature increase achieved in our experiment. As the maximum increase in temperature for a given pellet is predicted to be at its center, ΔT_{center} is expected to correlate with cytotoxic response. A comparison of the calculated ΔT_{center} for cell pellets containing variable cell numbers and iron concentrations with fractional survival confirms this expectation (Figures 5C & D). We find no evidence suggesting significant

thermally mediated cytotoxicity below a predicted ΔT_{center} of 4.4°C or absolute predicted core temperature of 41.4°C. Cytotoxicity trends with both measured $\Delta T_{surface}$ (Figure 5B) and calculated ΔT_{center} (Figure 5C) regardless of nanoparticle concentration or pellet size. This indicates that hyperthermia is the dominant cytotoxic factor in our experiment.

To address whether our theoretical model predicts local intracellular temperature elevations near the collections of internalized nanoparticles, we calculated the $\Delta T_{surface}$ of a 500-nm diameter cluster of BNF particles using Equation 4. The resulting value of 1.2×10^{-4}°C indicates that localized, intracellular temperature changes are unlikely to contribute to cytotoxicity.

Discussion

We have used a simple experimental model to evaluate the size dependence of AMF-mediated hyperthermia and its associated cytotoxicity using prostate cancer cells containing intracellular ferromagnetic nanoparticles. We observe that the maximum measured temperature increase at the surface of cell pellets is a function of both pellet size and particle concentration as would be expected from diffusive heat transfer. Finally we observe that the cytotoxicity associated with AMF treatment scales with this temperature increase and becomes negligible in small pellets as the achieved increase in cell-pellet temperature diminishes.

The relationship between cell-pellet size, intracellular particle concentration and cell-pellet surface temperature increase is well described by the solution for the heat diffusion equation as it is applied to the steady-state (as $t > \infty$) surface temperature increase of a uniformly and constantly heated spherical object existing in an infinite heat sink (Equation 4). Here, the uniform heating rate is treated simply as the product of the particle concentration and particle SLP (Equation 6). This agreement is remarkable considering the experimental system deviates significantly from the approximations used to derive Equation 4 in a number of ways. Significant deviations include: the intracellular particle distribution is not homogeneous, but is localized to vesicles as large as 500 nm in diameter (Figure 3D); the cell pellets are not spherical and possess significant asymmetry; cell membranes exist and separate the collections of nanoparticles; the peak change at the pellet surface temperature measured is assumed to be indicative of the change in temperature at $t = \infty$, although it is measured at a finite time (30 min) after initiating heating and the heat sink is not infinite but is comprised of 0.5 ml of medium, the vessel and the circulating water jacket within the solenoid.

Our interpretation of the above results is that both the thermal and associated cytotoxic effects of hyperthermia mediated by intracellular nanoparticles behave according to heat diffusion theory and are subject to the same overarching scaling effect as other forms of hyperthermia. In other words, macroscopic heat diffusion dominates even on the relevant length scales for cells. Namely, the smaller a system that is heated from within (at a given rate of energy deposition per unit volume), the smaller the temperature increase incurred by that system and consequently the smaller the cytotoxic effect of such heating. Thus, it is presently impossible to therapeutically heat a single cell by magnetically perturbing intracellular nanoparticles. In fact, in this study, the smallest cell pellet in which significant hyperthermia-mediated cytotoxicity was observed comprised 2.5×10^5 cells (containing Fe at a concentration of 200 pg Fe/cell). The correlation of cytotoxicity with measured temperature change indicates that hyperthermia contributes in a dominant fashion to cell toxicity in this experiment.

A number of experimental studies evaluating cytotoxicity mediated by AMF-treated intracellular particles in pellets of cells have been reported [3,9,22]. However, they fail to provide an explicit evaluation of the relationship between cytotoxicity and cell ensemble size. In aggregate these studies leave an unclear description of the relationship between intracellular and extracellular hyperthermia.

Kalambur and coworkers demonstrated a decrease in cell viability in prostate cancer cells loaded with iron oxide nanoparticles and heated while in pellet form by AMF and interpreted the cytotoxicity incurred as being due to a combination of effects from intracellular and extracellular nanoparticles [9]. While they provide a theoretical scaling analysis of heat-ability as a function of cell ensemble size based on a simple heat diffusion model, they do not experimentally address variations in either heatability or cytotoxicity with cell-pellet size.

Wilhelm and coworkers evaluated the relative cytotoxicity of iron oxide nanoparticle-loaded and -unloaded cells coexisting in a large (20 million cells) loose pellet and exposed to AMF [22]. They employed a single time point, flow cytometric measurement of propidium iodide to demonstrate equivalent relative propidium iodide uptake in nanoparticle-loaded and nanoparticle-empty cell populations. This result indicates that cytotoxic hyperthermia is a function of total iron particle content in the pellet, a finding consistent with the observations described here. These results also imply that a therapeutically significant temperature differential is not achieved between the cellular environments of transfected and untransfected cells. In short, their work supports the equivalency of intracellular and extracellular hyperthermia in terms of cytotoxic effect.

Jordan and coworkers attempted to compare intracellular and extracellular hyperthermia by comparing the clonogenic survival of nanoparticle-loaded cells treated in pellets by AMF with equivalent cell pellets treated by external water bath [3]. They attempted to apply equivalent thermal schedules by modulating the intensity of AMF to maintain the temperature of the pellet (as measured at a single location within the pellet) at a value equivalent to the temperature of the water bath. Their results indicated preferential cytotoxicity for intracellular heating when attempting to maintain treatment temperature at 43°C. However, they fail to account for temperature variation expected across the cell pellet, which is evident in the theoretical treatment provided here (Equation 3).

It is our position that a temperature measurement at a single location within an internally heated cell pellet is inadequate to assign thermal dose. We have also attempted to make this comparison by assigning a thermal isoeffective dose [23], based on the well known Arrhenius relationship, to both our AMF-treated cell pellets and equivalent pellets treated by water bath (data not shown). We employed the commonly used cumulative equivalent minutes at 43°C (CEM 43). However, this assignment was based on our temperature measurement at a single location on the pellet surface and did not adequately account for either the expected temperature gradient across the pellet or the dynamic nature of this gradient. We therefore feel that using this approach to compare the cytotoxicity of hyperthermia mediated by intracellular particles to externally applied heat is misleading. These limitations may explain the discrepancy in cytotoxicity observed by Jordan *et al.* [2,3,6].

In this work, we measure only the effects of intracellular hyperthermia, and we explore the size dependence of intracellular heating in terms of both thermal and cytotoxic effect. We have determined that this size dependence is remarkably well described by a simple model that ignores intercellular thermal barriers. We also confirm that the cytotoxicity associated with intracellular AMF-mediated heating becomes negligible in small collections of cells.

We explicitly demonstrate the minimum number of cells within a pellet required for cytotoxic hyperthermia to be achieved for a given concentration of particles having a specific SLP. It is noteworthy to mention that we do not address the convective heat transfer that would be present in vascularized tumors *in vivo*. We would expect a larger minimum size of tumor to be effectively heated in this setting. Further work is needed to compare these results with both external (interstitial) nanoparticle hyperthermia and with molecular-targeted (antibody) surface-bound nanoparticle hyperthermia. The latter case is particularly interesting in light of recently reported results [24].

Conclusion

Hyperthermia, mediated by intracellular magnetic nanoparticles, is subject to the same scaling effect as macroscopically induced hyperthermia. This scaling effect, resulting in effectively less heating in smaller systems, is predicted by simple heat diffusion theory. As a consequence, there is an effective 'smallest size' of tumor that can be treated by intracellular heating. This phenomenon is a practical barrier to applying nanoparticle-mediated hyperthermia to the treatment of micro-metastatic cancer.

Future perspective

Magnetic iron oxide nanoparticle hyperthermia is an exciting prospect as a cell-specific tool for widely disseminated or occult disease. Despite many unsuccessful attempts there is renewed interest due to the development of novel material formulations that are able to deliver high heat payloads for substantially less material or doses than was possible in previous decades. Clinical success of this modality for disseminated cancer can only be realized if the formulations demonstrate significantly reduced nonspecific uptake of the nanoparticles by nontargeted organs and tissues following systemic delivery; high specific accumulation in cancer tissue; and that the inherent limitations of this approach are acknowledged. Furthermore, the results of this work show that as a single-agent therapy targeted magnetic fluid hyperthermia is unlikely to succeed in the clinic. Thus, efforts must be directed to the development of this technology as part of a broad multimodality therapeutic platform that is designed to capitalize on the inherent advantages that heat therapy offers. Namely, heat is a powerful sensitizer for radiation and chemotherapies. These nanoparticulate platforms provide inherent advantages for the development of multifunctional nanoscale therapeutic devices. As demonstrated in this work, it is important to fully characterize these devices and to understand their inherent limitations.

Supplementary Material

Refer to Web version on PubMed Central for supplementary material.

Acknowledgments

The authors thank M Delannoy at the Johns Hopkins School of Medicine Election Microscopy core facility for help with transmission electron microscopy images.

References

Papers of special note have been highlighted as:

- ■ of interest
- ■■ of considerable interest

1■. Gordon RT, Hines JR, Gordon D. Intracellular hyperthermia. A biophysical approach to cancer treatment via intracellular temperature and biophysical alterations. Med Hypotheses. 1979; 5(1): 83–102. Relevant historical reference that first described the concept of intracellular hyperthermia as a potentially beneficial therapy. [PubMed: 459972]

2■. Jordan A, Wust P, Scholz R, et al. Magnetic fluid hyperthermia (MFH). Scientific and Clinical Applications of Magnetic Carriers. 1997:569–595. Good historical review of intracellular nanoparticle hyperthermia.

3. Jordan A, Schulz R, Wust P, et al. Endocytosis of dextran and silan-coated magnetite nanoparticles and the effect of intracellular hyperthermia on human mammary carcinoma cells *in vitro*. J Magn Magn Mater. 1999; 194(1–3):185–196.

4. Kita E, Oda T, Kayano T, et al. Ferromagnetic nanoparticles for magnetic hyperthermia and thermoablation therapy. J Phys D Appl Phys. 2010; 43(47):474011.

5. Gilchrist RK, Shorey WD, Hanselma RC, et al. Effects of electromagnetic heating on internal viscera: a preliminary to the treatment of human tumors. Ann Surg. 1965; 161:890–896. [PubMed: 14295940]

6. Jordan A, Wust P, Faehling H, et al. Inductive heating of ferrimagnetic particles and magnetic fluids: physical evaluation of their potential for hyperthermia. Int J Hyperthermia. 2009; 25(7):499–511. [PubMed: 19848612]

7■. DeNardo SJ, Denardo GL, Natarajan A, et al. Thermal dosimetry predictive of efficacy of ^{111}In-ChL6 nanoparticle AMF-induced thermoablative therapy for human breast cancer in mice. J Nucl Med. 2007; 48(3):437–444. Describes nanoparticle (magnetic fluid) hyperthermia following systemic intravenous infusion of antibody-targeted magnetic nanoparticles. [PubMed: 17332622]

8■■. Rabin Y. Is intracellular hyperthermia superior to extracellular hyperthermia in the thermal sense? Int J Hyperthermia. 2002; 18(3):194–202. One of several theoretical works describing magnetic nanoparticle hyperthermia limitations. The thermal model described in this manuscript is based upon Rabin's description. [PubMed: 12028637]

9■. Kalambur VS, Longmire EK, Bischof JC. Cellular level loading and heating of superparamagnetic iron oxide nanoparticles. Langmuir. 2007; 23(24):12329–12336. One of several theoretical works describing magnetic nanoparticle hyperthermia and limitations. [PubMed: 17960940]

10. Hergt R, Dutz S. Magnetic particle hyperthermia-biophysical limitations of a visionary tumour therapy. J Magn Magn Mater. 2007; 311(1):187–192.

11. Keblinski P, Cahill DG, Bodapati A, et al. Limits of localized heating by electromagnetically excited nanoparticles. J Appl Phys. 2006; 100(5):054305.

12■■. Yamada K, Oda T, Hashimoto S, et al. Minimally required heat doses for various tumour sizes in induction heating cancer therapy determined by computer simulation using experimental data. Int J Hyperthermia. 2010; 26(5):465–474. Recent work describing simulations of induction heating of cancer tumors. Provides a description of heat conduction and flow through tumors. [PubMed: 20377361]

13. Hergt R, d'Ambly CG, Andra W, et al. Physical limits of hyperthermia using magnetite fine particles. IEEE Trans Magn. 1998; 34(5):3745–3754.

14. Gruettner C, Mueller K, Teller J, et al. Synthesis and antibody conjugation of magnetic nanoparticles with improved specific power absorption rates for alternating magnetic field cancer therapy. J Magn Magn Mater. 2007; 311(1):181–186.

15■■. Dennis CL, Jackson AJ, Borchers JA, et al. Nearly complete regression of tumors via collective behavior of magnetic nanoparticles in hyperthermia. Nanotechnology. 2009; 20(39):395103. Describes physical and magnetic properties of the particles used for experiments described in the current manuscript. [PubMed: 19726837]

16■■. Bordelon D, Cornejo C, Gruettner C, DeWeese TL, Ivkov R. Magnetic nanoparticle heating efficiency reveals magneto-structural differences when characterized with a wide ranging and high amplitude alternating magnetic field. J Appl Phys. 2011; 109:124904. Provides heating data and a description of methods to measure heating data of the particles used in the current manuscript.

17. Ivkov R, Mallipudi R, Kumar A, Deweese T. AMF shielding reduces non-specific tissue heating for magnetic nanoparticle therapy. Int J Rad Onc: Biol Phys. 2010; 78(S658 Suppl S)

18. Ivkov R, Mallipudi R, Kumar A, DeWeese TL. AMF shielding reduces non-specific tissue heating for magnetic nanoparticle therapy. Int J Rad Onc Biol Phys. 2010; 78(Suppl S):S658.

19. Bordelon D, Goldstein R, Nemkov V, et al. Modified solenoid coil that efficiently produces high amplitude AC magnetic fields with enhanced uniformity for biomedical applications. IEEE Trans Magn. 2012; 48(1):47–52.

20■■. Balasubrumanian T, Bowman HF. Temperature field due to a time-dependent heat source of spherical geometry in an infinite medium. J Heat Trans-T ASME. 1974; 96(3):296–299. Description of the basic heat transfer model (sphere in a conductive medium) used in this manuscript.

21. Andra W, d'Ambly CG, Hergt R, et al. Temperature distribution as function of time around a small spherical heat source of local magnetic hyperthermia. J Magn Magn Mater. 1999; 194(1–3):197–203.

22. Wilhelm C, Fortin J-P, Gazeau F. Tumor cell toxicity of intracellular hyperthermia mediated by magnetic nanoparticles. J Nanosci Nanotechnol. 2007; 7:2933–2937. [PubMed: 17685322]

23. Dewey WC. Arrhenius relationships from the molecule and cell to the clinic. Int J Hyperthermia. 2009; 25(1):3–20. [PubMed: 19219695]

24■. Creixell M, Bohórquez AC, Torres-Lugo M, Rinaldi C. EGFR-targeted magnetic nanoparticle heaters kill cancer cells without a perceptible temperature rise. ACS Nano. 2011; 5:7124–7129. Report of *in vitro* cytotoxicity in cells containing membrane-bound and internalized antibody-labeled magnetic nanoparticles following alternating magnetic field exposure. Cytotoxic response was observed at power and heating conditions that failed to produce a measureable temperature increase to hyperthermic levels. Comparison of the results reported by Creixell *et al.* with those presented here underscores the point that further systematic studies are needed. [PubMed: 21838221]

Executive summary

- Here, hyperthermia was achieved by the intracellular Bionized NanoFerrite nanoparticles exposed to alternating magnetic fields.
- The maximum measured surface temperatures of cell pellets treated by alternating magnetic fields agree well with those predicted by a simple heat diffusion model that ignores intercellular thermal barriers.
- Cytotoxicity scales with measured cell-pellet surface temperature and becomes negligible in small pellets.
- The smallest cell pellet in which hyperthermia-mediated cytotoxicity was observed in our experiment contained 250,000 cells with an intracellular iron concentration of approximately 200 pg Fe/cell.
- Our results demonstrate a practical dosimetric barrier to treating small micro-metastatic tumor foci with intracellular hyperthermia.

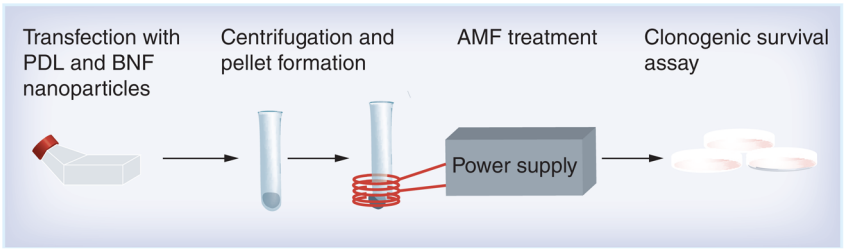

Figure 1. Experimental design

Schematic showing the experimental design: from left to right, DU145 cells are loaded in culture flasks with starch-coated BNF nanoparticles and PDL. Cell pellets are formed by centrifugation. The pellets are treated by AMF. AMF-treated and untreated cells are plated and fractional survival determined by clonogenic assay.

AMF: Alternating magnetic field; BNF: Bionized NanoFerrite; PDL: Poly-D-Lysine.

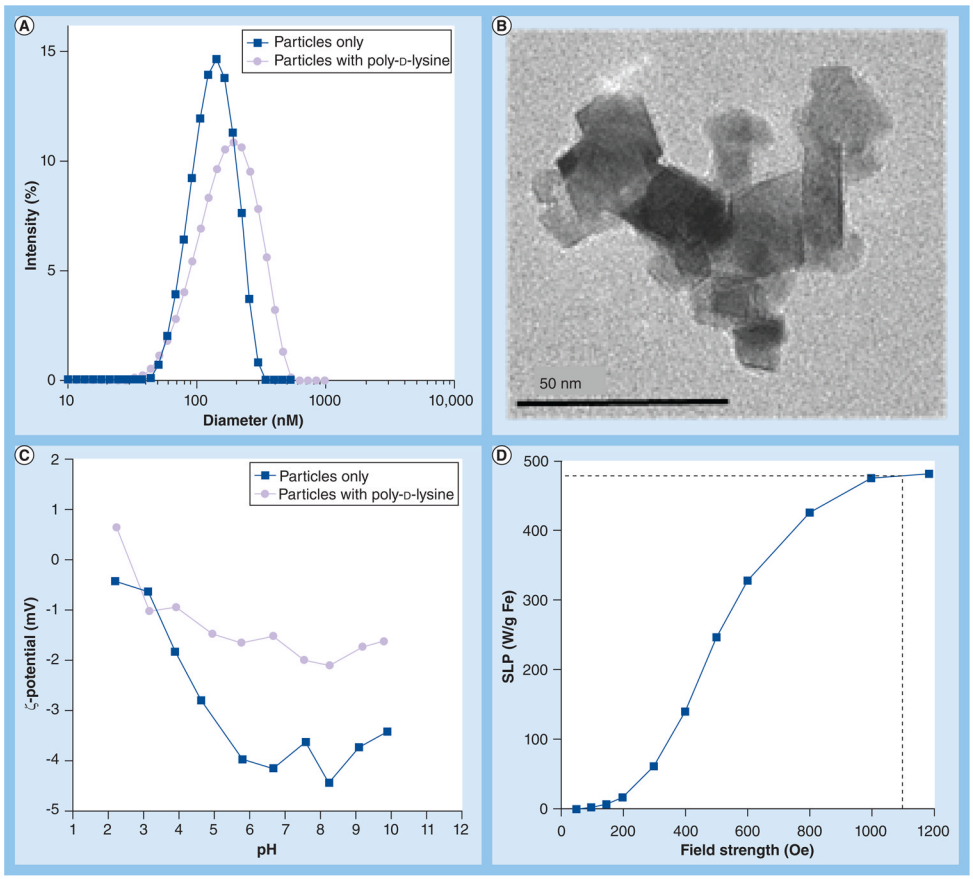

Figure 2. Particle characteristics

(A) Particle size. Photon correlation spectrograph (PCS) showing mean hydrodynamic diameter of starch-coated BNF particles in phosphate-buffered saline (PBS) and PBS with PDL. **(B)** Particle transmission electron microscopy. Magnetic core of a particle comprising multiple crystals. **(C)** Particle ζ-potential. The ζ-potential of starch-coated BNF particles either in PBS or PBS with PDL is shown as a function of pH. **(D)** Particle SLP. Vertical dashed line indicates field amplitude used in study.

BNF: Bionized NanoFerrite; PDL: Poly-D-lysine; SLP: Specific loss power.

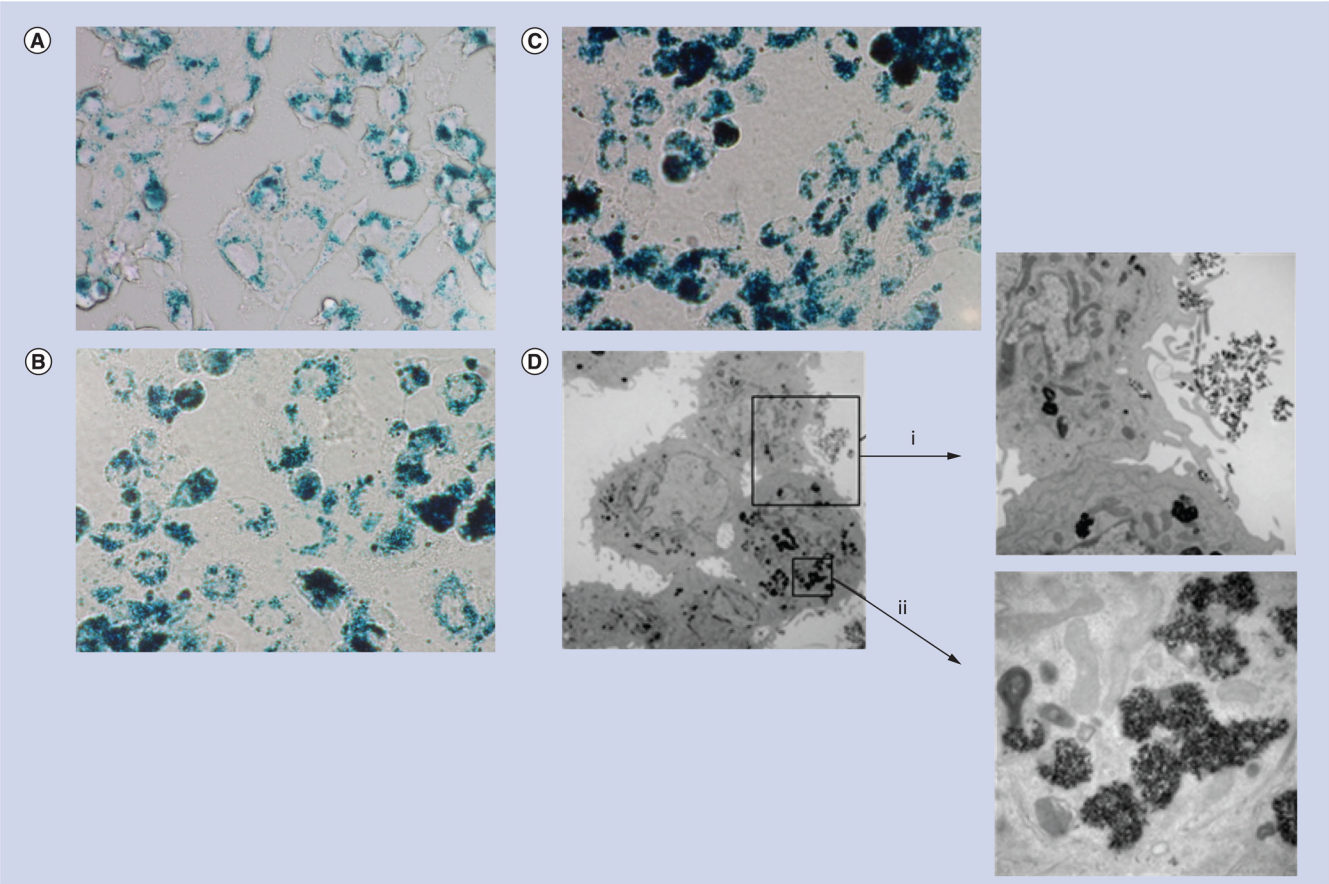

Figure 3. Microscopy images of DU145 cells containing nanoparticles

(A–C) Light micrographs (color, 40×). Cell samples were treated under conditions (listed in Table 1) corresponding to **(A)** 70 pg Fe/cell, **(B)** 105 pg Fe/ cell and **(C)** 200 pg Fe/cell. They were fixed and stained with Prussian Blue to highlight iron deposits. **(D)** Transmission electron micrographs under similar conditions as **(A)**. Magnifications are: 4000×, inset (i) 12,000×, and inset (ii) 40,000×. Note that the intracellular nanoparticle distribution is inhomogeneous, with cells appearing to phagocytize particle clusters (i) that are further concentrated within intracellular compartments or endosomes (ii).

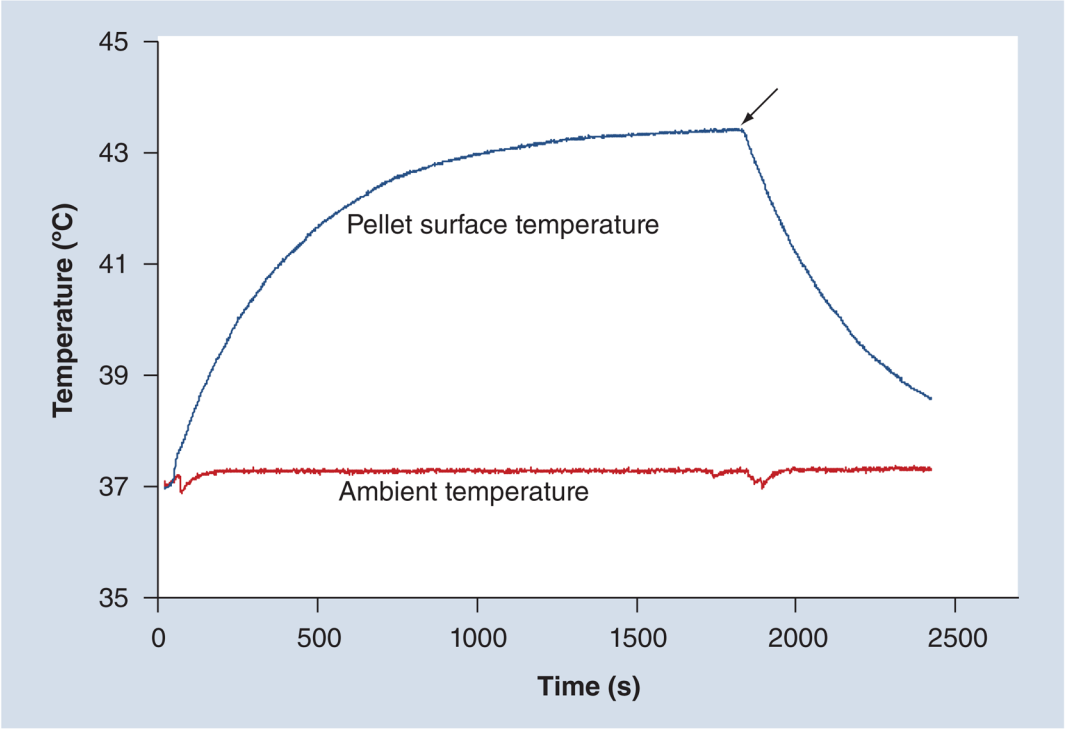

Figure 4. Dynamic temperature profile of cell pellet

Measured surface temperature profile during alternating magnetic field treatment for a 500,000 cell cluster with an iron content of 199 pg/cell (cells were allowed to equilibrate to 37°C in sample chamber for 10 min before the power was turned on; the arrow indicates when the power was turned off).

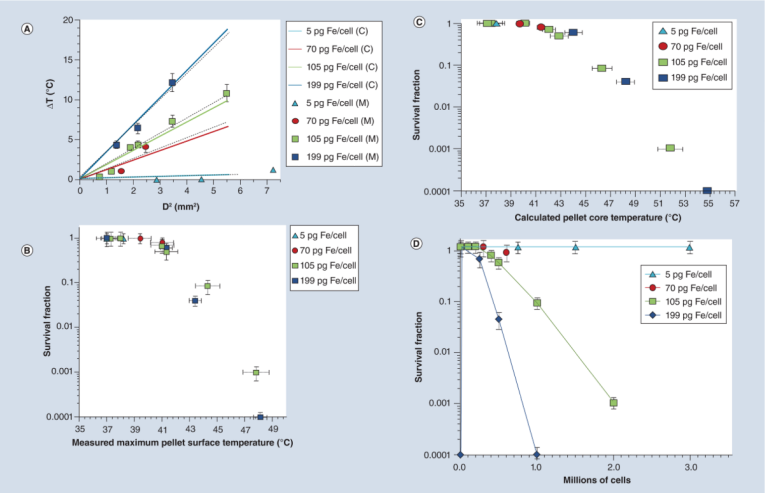

Figure 5. Thermometry and cell survival results

(A) Comparison of the measured maximum change of cell pellet surface temperature (markers, M = Measured) versus the square of the diameter, D^2, with calculated maximum cell pellet surface temperature using Equation 4 in the text (solid lines, C = Calculated) for cell pellets with different intracellular iron concentrations. The dashed lines indicate linear least square fits of measured data with R^2 values of 0.99, 0.96 and 0.99 corresponding to 70, 105 and 199 pg of Fe/cell, respectively. **(B)** Fractional survival of cells from alternating magnetic field-treated pellets as a function of their measured pellet surface temperature. **(C)** Surviving fraction of DU145 containing Bionized NanoFerrite nanoparticles versus calculated cell-pellet core temperature. **(D)** Surviving fraction of DU145 containing Bionized NanoFerrite nanoparticles versus cell number separated by level of intracellular iron concentration. Error bars refer to standard error of the mean of measured values.

Table 1

Uptake of BNF nanoparticles by DU145 prostate cancer cells measured by ICP-MS.

Fe/PDL (μg/ml)†	Average Fe (pg/cell) ± SD	Estimated particle number/cell	n‡
0/1.5	<0.01	<8.4	6
150/0	2.5 ± 0.6	2100	4
15/0.5	4.5 ± 1.3	4000	8
75/1	69.7 ± 21.8	58,500	5
100/1.5	104.5 ± 6.9	87,800	6
150/1.5	199.1 ± 41.5	167,200	4

† Final concentration in the media of either Fe or PDL.

‡ Number of samples from similar treatments that were subjected to inductively coupled plasma mass spectrometry analysis.

PDL: Poly-D-lysine; SD: Standard deviation.

Table 2

Iron concentration, cell number and maximum measured temperature at the surface of DU145 cell pellets treated by alternating magnetic field.

Iron concentration (pg Fe/cell)	Cell number (cells per pellet)	Maximum measured surface temperature (°C)
5	750,000	37.0
	1,500,000	37.0
	3,000,000	38.2
70	300,000	39.4
	600,000	41.0
105	1000	37.0
	10,000	37.0
	100,000	37.3
	200,000	38.0
	400,000	41.0
	500,000	41.3
	1,000,000	44.3
	2,000,000	47.8
	10,000	37.0
199	250,000	41.3
	500,000	43.4
	1,000,000	49.1